Effective compressive elastic behavior of rhombic dodecahedron structure with and without border constraints

Boning Yu, Yuming Li, Boussad Abbes, Baoyi Yu, Shujun Li

Version of Record: https://www.sciencedirect.com/science/article/pii/S0263822320334292
Manuscript_2eed6d6996172076ff02f0fdfef4499c

Effective Compressive Elastic Behavior of Rhombic Dodecahedron Structure with and without Border Constraints

Boning Yu[1,2], Yuming Li[1,*], Boussad Abbes[1], Baoyi Yu[2], Shujun Li[3]

[1] Lab. MATIM, Université de Reims Champagne-Ardenne, Reims, France
[2] Shenyang University of Technology, China
[3]Institute of Metal Research, Chinese Academy of Sciences, China
Email: yuming.li@univ-reims.fr

Abstract

The effective compressive elastic modulus of the cellular rhombic dodecahedron structure, with $m \times n$ cells in the X- and Y- directions in matrix, has been studied. The effective compressive elastic modulus of the structure without border constraint is a function of m and n; while for the structure with border constraints in the X- and Y- directions it is found unique that is independent of m and n, and is a function of the porosity of the structure. In order to study and understand the range of the effective compressive elastic modulus for the structure without border constraint with explicit expression of the structure parameters, an analytical model has been developed to evaluate the lower and upper bounds. The analytical model is also valid for the structure with double border constraints with a unique modulus. In addition, a finite element method based on beam theory in neglecting shearing effect has been developed for both cases, under the specific boundary conditions used in a unit cell, including finite and infinite numbers of cells m or/and n.

As such, the analytical method based on beam theory takes into consideration the finite geometry dimensions and the fictive infinite geometry dimensions. The later gives the upper bound of the effective compressive elastic modulus. The modulus of the structure composed of finite numbers of cells $m \times n$ without border constraint is not only a function related to the porosity of the structure, but the geometrical parameters d and b. An experimental test has been fulfilled and compared to the theoretical one with reasonable agreement.

1. Introduction

With the continuous and quick growing of industrial demands, the product design diversification and structural complexity have become a prevailing trend. And the porous structure composed of a network of interconnected solid struts or flat plates that form the edges and faces of the unit, has become one of the promising products [1]. It can achieve complex shape changes to satisfy the product performance requirements. For example, according to different mechanical properties and shape requirements in multiple directions, the porous structure can be manipulated within the controllable range to provide resultantly different structural stiffness, shock resistance, and high energy absorption [2-5].

With the quick development of additive manufacturing technology, the functionally graded porous structures can be customizable and efficiently manufactured. Moreover, these structures have been widely used in a variety of fields according to their performance diversity, such as unmanned aerial vehicle [6], aerospace [7], and biomedical [8-9].

Due to its design characteristics, the functionally graded porous structure is suitable for topologically optimization method or periodic arrangement [10-11]. The most typical periodic

structure includes a two-dimensional array of polygons such as the honeycomb structure [12], or a three-dimensional structure composed of struts [13] or layers [14].

Among the above-mentioned porous structures, the rhombic dodecahedron is often employed for biomedical application as the substitute for human bones grace to its similarity of porosity and density with natural human bones. Additionally the low elastic modulus avoids the stress shielding effect and makes it safer as a substitute for human bones [15]. Meanwhile, titanium alloy, especially Ti6Al4V alloy, is suitable as an implant material to replace human bones due to its advantages in excellent mechanical performance, corrosion resistance, and biocompatibility. As the porosity increases and the elastic modulus decreases, Ti6Al4V functional porous structural material implants will fasten the rate of tissue generation and integration. Compared to the traditional cast or forged products, Ti6Al4V biomedical samples prepared by EBM (Electron beam melting) have no significant differences in various mechanical properties [16-18].

In recent years, plentiful researches have been done to the rhombic dodecahedron porous structures materials fabricated by additive manufacturing. Generally, it was quite challenging to study and understand the mechanical properties of three-dimensional rhombohedral dodecahedron porous materials. The experimental method, FE modeling and analytical models have been used in the research works.

Cao et al. [19] have proposed a new modified rhombohedral dodecahedron porous structure by redefining the cross section of the original struts with an optimizable shape parameter.
Yang et al. [20] have constructed samples by additive manufacturing with periodical arrangement of rhombic dodecahedrons in three directions, and have found the increase in the size of the unit cell leads to a decrease in the printability, Young's modulus, yield strength, and energy absorption capability.

Horn et al. [21] have verified that the flexural modulus and ultimate strength were well fitted to the Gibson-Ashby relation by conducting four-point flexure tests on Ti6Al4V prismatic bars composed of a rhombic dodecahedron prepared by EBM.

For artificial bone implant, the effective compressive elastic behavior of the structure is a very important factor. The porous Ti6Al4V alloys is a medical friendly material for the bone implant applications because its compressive properties can be quantitatively tailored by the porosity in order to be compatible with trabecular bone both on the quasi-static condition and in the range of physiological strain rate, as Young's modulus and the strain rate are found to be related to the porosity [22]. In the present work, focused attentions have been paid to study the elastic properties of the rhomboidal dodecahedron structure under compression.

In the application of the rhombic dodecahedron structure in the implant, the numerical modelling of the structure is too tedious and time consuming due to the complexity of the structure. The homogenization of the structure under compression enables to obtain an equivalent homogeneous solid with an effective elastic modulus in the compression direction that will make the numerical simulations much more efficient.

Babaee et al. [23] have derived analytical relationships for the effective mechanical properties of an open rhomboidal dodecahedron unit cell and tessellated cellular structure with periodic boundary conditions by using fundamental concepts of mechanics of materials. In this study, the rhomboidal dodecahedron structure is supposed to be periodic with infinite geometry dimension, and the effective elastic modulus has been expressed as a function of the porosity, without taking into consideration the real dimension of the structure. In fact, the effective elastic modulus may not be a function purely related to the porosity, but may be related to the dimension of the structure too

according to different application conditions of the structure. When the structure has no border constraint, the effective elastic modulus changes gradually from the lower bound to the upper bound as the number of cells varies from one to infinite. Only in the case with infinite number of cells, the effective elastic modulus is a function of porosity. And when the structure has border constraint in the *X*- and *Y*- directions in the plane, the effective elastic modulus is a function of porosity, not regarding the numbers of cells.

In the present study, an analytical modeling and FE method based on the beam theory have been developed to reveal the compressive effective elastic modulus of the rhomboidal dodecahedron. A perfect agreement has been achieved between the results of the analytical model and those of FE method.

2. Methodology

The mechanical properties of the cellular rhombic dodecahedron structure under compression in the vertical direction will be studied as shown in Fig. 1.A. The structure is based on the rhombic dodecahedron and supposed to be composed of $m \times n \times l$ identical cellular cells. As shown in Fig. 1.B, one unit cell of the structure is a cubic space containing an entire rhombic dodecahedron of 24 struts and 8 struts connected to its neighbor cells in all the three directions. This is different from the structure whose unit cell volume contains entire rhombic dodecahedrons due to the range choice of rhombic dodecahedron's direction. As the number of layers l in the vertical direction does not influence the effective elastic modulus in this direction, l is supposed to be 1 without losing the generality. Therefore the structure with $m \times n$ cells will be studied and the number of rows m and the columns n varies theoretically and mathematically from 1 to infinite. The effective elastic modulus of the structure in the vertical direction is a function of m and n. One unit cell gives the lower bound of the effective elastic modulus and a structure with infinite numbers of cells in row ($m \to \infty$) or/and in column ($n \to \infty$) gives the upper bounds for one direction (row or column) or the upper bound for two directions (row and column).

Two different cases of application conditions of the rhombic dodecahedron structure under compression will be studied: 1) without border constraint in the the *X*-direction and the *Y*-direction; 2) with border constraint in the the *X*-direction and the *Y*-direction.

The analytical method and finite element (FE) method both based on beam theory will be used to predict the effective modulus: each strut is considered as a beam. As the analytical and the FE methods are based on the same theory, these two methods will give the same results. Therefore the analytical method is only chosen to calculate the bounds without constraint and the case with border constraint that doesn't need much manual calculation. That is, the analytical method will be used to calculate the lower bound ($m=n=1$) and upper bound for two directions ($m \to \infty$; $n \to \infty$) of the effective elastic modulus for case 1) and the bulking elastic strength for case 2); the FE method will be used to calculate any value of m and n for case 1) due to its calculation capacity that can establish the graphic of the effective elastic modulus related to m and n. For the upper bound due to the infinite number of rows or/and columns, special boundary conditions will be applied with the minimum number of cells in both analytical and the FE methods.

2.1 Geometry of the unit cell

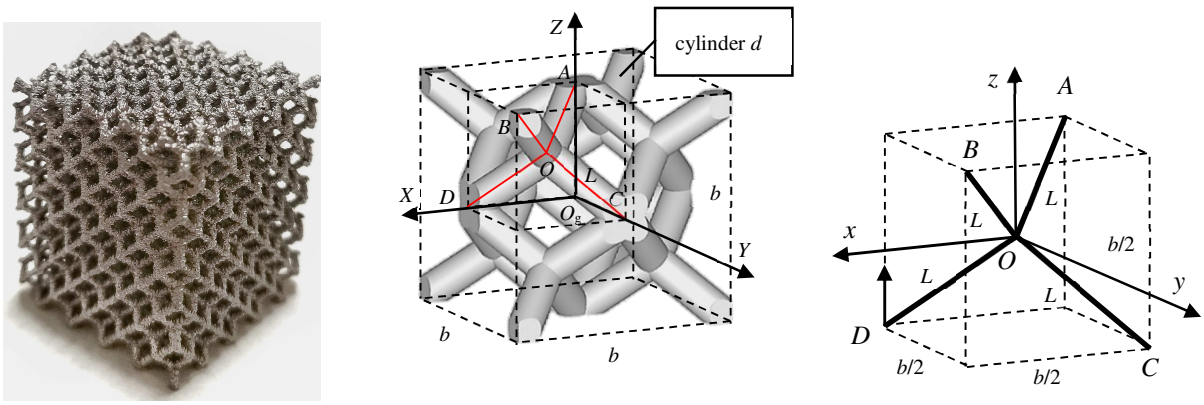

A) Fabricated structure B) Unit cell C) 1/8 of a unit cell

Fig. 1. Cell of rhombic dodecahedron structure

As shown in Fig. 1.B, a unit cell based on the rhombic dodecahedron is composed of 32 cylinder struts with the diameter d and length L for each. This cell is framed by a cubic box with the edge length b.

1/8 of a unit cell in a cubic box is taken for the analysis of the upper and lower bounds of the effective elastic modulus due to its triple symmetric geometry. The length of the beam L and the edge length of the box b holds:

$$L = \frac{\sqrt{3}}{4} b \tag{1}$$

As shown in Fig. 1.B and 1.C, the local coordinate system O-xyz shares the same directions of X-, Y- and Z-axe in the global coordinate system attached at the center of the cubic box point O_g. In the 1/8 of the unit cell shown in Fig. 1.C, the coordinates of the nodes in the local coordinate system O-xyz are as follows:

$$A(-a,-a,a),\ B(a,a,a),\ C(-a,a,-a),\ D(a,-a,-a) \tag{2}$$

with $a = L/\sqrt{3}$.

And for each beam i (i = A, B, C, D), a local coordinate system attached to the origin point O is established and its directional vectors on the axes are designed as $\vec{n}_i$, $\vec{t}_{i1}$ and $\vec{t}_{i2}$, respectively. The normal vector $\vec{n}_i$ of the beam's section is given by:

$$\vec{n}_i = norm\left(\overrightarrow{Oi}\right) \tag{3}$$

where the normalization function $norm()$ is defined as:

$$norm\left(\vec{u}\right) = \vec{u} / \left\|\vec{u}\right\|$$

By using Eqs. (2) and (3), the normal directions of the beams are numerically expressed as:

$$\vec{n}_A = \frac{1}{\sqrt{3}}\begin{Bmatrix}-1\\-1\\1\end{Bmatrix},\ \vec{n}_B = \frac{1}{\sqrt{3}}\begin{Bmatrix}1\\1\\1\end{Bmatrix},\ \vec{n}_C = \frac{1}{\sqrt{3}}\begin{Bmatrix}-1\\1\\-1\end{Bmatrix},\ \vec{n}_D = \frac{1}{\sqrt{3}}\begin{Bmatrix}1\\-1\\-1\end{Bmatrix} \tag{4}$$

Two tangential vectors perpendicular to $\vec{n}_i$ for beam i (i = A, B, C, D) are chosen as follows:

$$\vec{t}_{i1} = norm\left(\left(\vec{k}\cdot\vec{n}_i\right)\vec{n}_i - \vec{k}\right),\quad \vec{t}_{i2} = \vec{n}_i \times \vec{t}_{i1}; \tag{5}$$

The vectors $\vec{n}_i, \vec{t}_{i1}, \vec{t}_{i2}$ serve as unit directional vectors in the three dimensions of the local coordinate system of beam *i*.

By using Eqs. (4) and (5), the directional vectors of the beams are numerically determined as:

$$\vec{t}_{A1} = \frac{1}{\sqrt{6}}\begin{Bmatrix}-1\\-1\\-2\end{Bmatrix},\quad \vec{t}_{A2} = \frac{1}{\sqrt{2}}\begin{Bmatrix}1\\-1\\0\end{Bmatrix};\ \vec{t}_{B1} = \frac{1}{\sqrt{6}}\begin{Bmatrix}1\\1\\-2\end{Bmatrix},\quad \vec{t}_{B2} = \frac{1}{\sqrt{2}}\begin{Bmatrix}-1\\1\\0\end{Bmatrix};$$

$$\vec{t}_{C1} = \frac{1}{\sqrt{6}}\begin{Bmatrix}1\\-1\\-2\end{Bmatrix},\quad \vec{t}_{C2} = \frac{1}{\sqrt{2}}\begin{Bmatrix}-1\\-1\\0\end{Bmatrix};\ \vec{t}_{D1} = \frac{1}{\sqrt{6}}\begin{Bmatrix}-1\\1\\-2\end{Bmatrix},\quad \vec{t}_{D2} = \frac{1}{\sqrt{2}}\begin{Bmatrix}1\\1\\0\end{Bmatrix}. \tag{6}$$

It's worth mentioning that with this choice, the directional vectors $\vec{t}_{A1}$, $\vec{t}_{B1}$, $\vec{t}_{C2}$ and $\vec{t}_{D2}$ are in the symmetric plane $X=Y$ which coincides well with the double symmetry and will simplify the expression of forces and moments both in the global and in the local coordinate system.

2.2 Application conditions of the structure under compression

Two cases of application conditions of the structure under compression exist: the borders of the structure are under constraint in the *X*-direction or/and the *Y*-direction or not. When the borders are only under constraint in one direction (*X*- or *Y*-direction), the effective elastic modulus increases considerably with respect to that without constraint.

1) Application without border constraint in the plane XO_gY

If the structure has no border constraint in the plane XO_gY, all borders are free and the effective elastic modulus can be calculated related to the number of rows *m* and that of columns *n*. The effective elastic modulus of the structure may be solved by beam theory without considering the shear efforts by using the FE method as a preference due to its strong calculation capacity. When *m* or/and *n* tend to infinite, the elastic behaviors of the cells become periodic, with non-zero horizontal displacement in the constrained direction on the borders of each cell, and special boundary conditions will be applied to the structure by using the minimum number of cells.

Particularly, the analytical method may be also used due to its simplicity in the analysis of the structure with one single unit cell without constraint in the plane XO_gY.

2) Application with border constraint in the plane XO_gY

For a structure under compression in the vertical direction, when the borders of the structure are constrained by two rigid panels, in the *X*-direction for example (left and right), the structure is periodic in the *X*-direction. In this case *m*×*n* cells (Fig. 2.A) and *m*×1 cells (Fig. 2.B) have the same elastic behavior, therefore one border-constrained structure of *m*×1 cells can present the border-constrained structure of *m*×*n* cells with any value of *n*. Different from the periodicity of the precedent case without constraint, the displacement in the constrained direction on the borders of each unit cell is zero.

If the structure is constrained in the *Y*-direction at the same time, 1×1 cell has the same effective elastic modulus in the vertical direction as that of *m*×*n* cells with any value of *m* and *n*.

The FE method is a preferential tool to calculate the effective elastic modulus for the structure with border constraint, but the effective elastic modulus in this case will be calculated by the analytical method too. Because the analytical method gives an explicit expression that allows a better understanding of the effective elastic modulus.

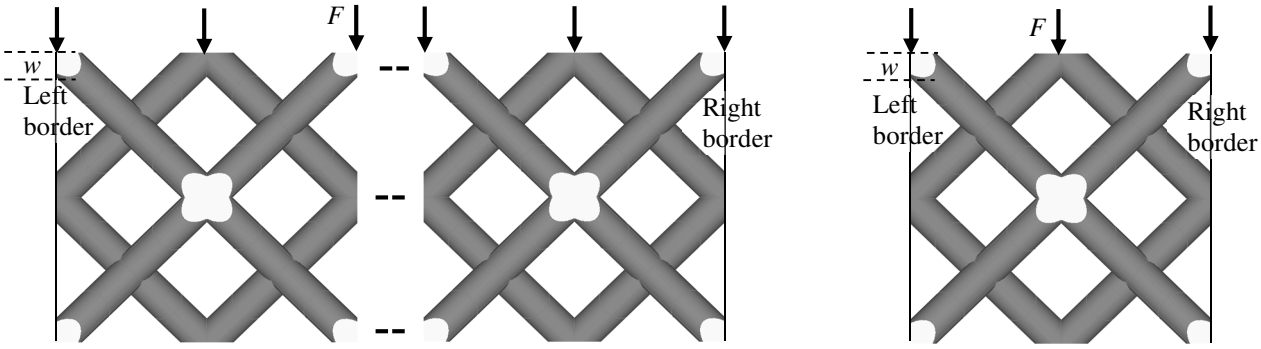

A) Structure of $m \times n$ cells B) Structure of $m \times 1$ cells

Fig. 2. Presentation of structure under compression

2.3 Lower and upper bounds of effective elastic modulus by using analytical method

Due to the triple symmetry of the structure, 1/8 of the unit cell is taken to calculate the lower and upper bounds of the effective elastic modulus in the *Z*-direction by using the beam theory in taking into consideration the tension, bending and torsion but neglecting the shearing effect with proper boundary conditions. A unit cell under vertical compression with free borders gives the lower bound of the effective elastic modulus in the *Z*-direction, in which $m=n=1$ as shown in Fig. 3.A and the case $m \to \infty$ and $n \to \infty$ gives the upper bound as shown in Fig. 3.B.

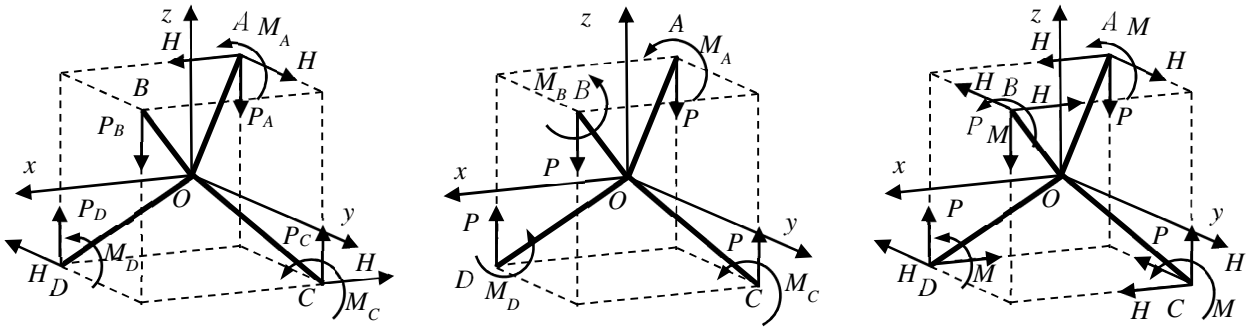

A) Modeling for 1×1 cell B) Modeling for $\infty \times \infty$ cells C) Modeling for border constraint

Fig. 3. Modeling for dodecahedron structure with $m \times n$ cells

In both cases with free borders and the case with border constraint, the equilibrium of forces holds:

$$\sum \vec{F}_{\text{ext}} = \vec{P}_A + \vec{P}_B + \vec{P}_C + \vec{P}_D = \vec{0} \tag{7A}$$

and that of moments at point *O* holds:

$$\sum \vec{M}_{/O} = \vec{M}_A + \vec{M}_B + \vec{M}_C + \vec{M}_D + L\vec{n}_A \times \vec{P}_A + L\vec{n}_B \times \vec{P}_B + L\vec{n}_C \times \vec{P}_C + L\vec{n}_D \times \vec{P}_D = \vec{0} \tag{7B}$$

1) *Modeling for lower bound of effective elastic modulus*

1/8 of the unit cell is taken in study and the global displacements U, V, W, θ or local displacements u, v, w, θ are taken as unknown variables. In the global coordinate system, by considering the triple

geometrical symmetry plane and the imposed displacement W in the Z-direction at the points A and B, the constant displacement boundary conditions hold as shown in Table 1:

point A	$U_A = V_A = 0;\ W_A = W;\ \theta_{Ax} = \theta_{Ay} = \theta_{Az} = 0$	point B	$W_B = W$
point C	$U_C = W_C = 0;\ \theta_{Cx} = \theta_{Cy} = \theta_{Cz} = 0$	point D	$V_D = W_D = 0;\ \theta_{Dx} = \theta_{Dy} = \theta_{Dz} = 0$

Table 1. Displacement boundary conditions:

As four beams share the same origin point O and the connection between any two beams are rigid-rigid, the complementary non-constant displacement boundary conditions are:

$$\vec{\theta}_{OA}(0) = \vec{\theta}_{OB}(0) = \vec{\theta}_{OC}(0) = \vec{\theta}_{OD}(0)$$

By considering the double symmetry of the unit cell in the plane XO_gY and the equilibrium shown in Eq. (7A), the forces on the 1/8 of the unit cell are supposed to be as shown in Fig. 3.A. In detail, as the points A and B are in the symmetric plane X=Y and point B is free in the X-direction *and* the Y-direction, $\vec{P}_A$ and $\vec{P}_B$ are supposed to be:

$$\vec{P}_A = \begin{Bmatrix} H \\ H \\ -P_A \end{Bmatrix},\ \vec{P}_B = \begin{Bmatrix} 0 \\ 0 \\ -P_B \end{Bmatrix} \tag{8A}$$

$\vec{P}_C$ and $\vec{P}_D$ share the same force in the Z-direction because the points C and D are symmetric with respect to the plane X=Y; And as the points A and C are in the symmetric planes X=0, thus $\left(\vec{P}_A + \vec{P}_C\right)\cdot\vec{i} = 0$, and as the points A and D are in the symmetric planes Y=0, thus $\left(\vec{P}_A + \vec{P}_D\right)\cdot\vec{j} = 0$, therefore $\vec{P}_C$ and $\vec{P}_D$ are supposed to be as follows as to satisfy the equilibrium Eq. (7A):

$$\vec{P}_C = \begin{Bmatrix} -H \\ 0 \\ (P_A + P_B)/2 \end{Bmatrix},\ \vec{P}_D = \begin{Bmatrix} 0 \\ -H \\ (P_A + P_B)/2 \end{Bmatrix} \tag{8B}$$

And still by using the triple symmetry, the exterior moments on the boundary nodes are supposed to be:

$$\vec{M}_A = \begin{Bmatrix} M_{Ax} \\ -M_{Ax} \\ 0 \end{Bmatrix},\ \vec{M}_B = \vec{0},\ \vec{M}_C = \begin{Bmatrix} M_{Cx} \\ M_{Cy} \\ M_{Cz} \end{Bmatrix},\ \vec{M}_D = \begin{Bmatrix} -M_{Cy} \\ -M_{Cx} \\ -M_{Cz} \end{Bmatrix} \tag{9}$$

In Eqs. (8A), (8B) and (9) there are in total 7 unknown variables. By using Eqs. (4), (8A), (8B) and (9) in Eq. (7B), Eq. (7B) is simplified as follows:

$$\left[\sqrt{2}\left(M_{Ax} + M_{Cx} - M_{Cy}\right) + \frac{\sqrt{6}}{3}\left(P_A - P_B - 2H\right)L\right]\vec{t}_{A2} = \vec{0} \tag{A-1}$$

The simplified moment equilibrium Eq. (A-1) indicates that the bending moment components (the sum is zero) are only in the $\vec{t}_{A2}$ direction that is perpendicular to the symmetric plane X=Y. Thus Eq. (A-1) is degraded to be a scalar equation.

For the beams OA and OB, by using the Eqs. (4), (8A), $\vec{M}_A$ and $\vec{M}_B$ in Eq. (9), the moments in the beam's section at distance s from O can be expressed respectively as:

$$\vec{M}_{OA}(s)=\vec{M}_A+(L-s)\vec{n}_A\times\vec{P}_A=\left[\sqrt{2}M_{Ax}-\frac{\sqrt{6}}{3}(P_A-H)(s-L)\right]\vec{t}_{A2} \tag{10A}$$

and

$$\vec{M}_{OB}(s)=\vec{M}_B+(L-s)\vec{n}_B\times\vec{P}_B=-\frac{\sqrt{6}}{3}P_B(s-L)\vec{t}_{B2} \tag{10B}$$

Eqs. (10A) and (10B) show that in a section of the beams *OA* and *OB*, there are only bending moments in $\vec{t}_{A2}$ and $\vec{t}_{B2}$ directions, respectively.

For beam *OA*, the displacement $y_{OA}(s)$ in the $\vec{t}_{A1}$ direction caused by the moment in the $\vec{t}_{A2}$ direction in Eq. (10A) holds:

$$EIy''_{OA}(s)=\sqrt{2}M_{Ax}-\frac{\sqrt{6}}{3}(P_A-H)(s-L) \tag{11A}$$

And two successive integrations of the above equation give:

$$EIy'_{OA}(s)=\sqrt{2}M_{Ax}s-\frac{\sqrt{6}}{6}(P_A-H)(s-L)^2+C_A \tag{11B}$$

and

$$EIy_{OA}(s)=\frac{\sqrt{2}}{2}M_{Ax}s^2-\frac{\sqrt{6}}{18}(P_A-H)(s-L)^3+C_As+D_A \tag{11C}$$

It is assumed that in the local coordinate system of each beam, the original point *O* doesn't move, that is, the local displacement is 0.

For beam *OA* there is no rotation at point *A* as shown in Table 1. Therefore the following two boundary conditions hold:

$$y_{OA}(0)=y'_{OA}(L)=0 \tag{B1-1}$$

By using the above two boundary conditions in Eqs. (11B) and (11C), the unknown coefficients C_A and D_A can be found and then these two Eqs. are rewritten as follows:

$$EIy'_{OA}(s)=\sqrt{2}M_{Ax}(s-L)-\frac{\sqrt{6}}{6}(P_A-H)(s-L)^2 \tag{11B_1}$$

$$EIy_{OA}(s)=\frac{\sqrt{2}}{2}M_{Ax}s(s-2L)-\frac{\sqrt{6}}{18}(P_A-H)\left[(s-L)^3+L^3\right] \tag{11C_1}$$

By using Eq. (11B_1) the rotation vector of beam *OA* at point *O* is expressed as:

$$\vec{\theta}_{OA}(0)=y'_{OA}(0)\vec{t}_{A2}=\frac{1}{EI}\left[-M_{Ax}L-\frac{\sqrt{3}}{6}(P_A-H)L^2\right]\begin{Bmatrix}1\\-1\\0\end{Bmatrix} \tag{12}$$

And for beam *OB*, the displacement $y_{OB}(s)$ in the $\vec{t}_{B1}$ direction and the moment in the $\vec{t}_{B2}$ direction given in Eq. (10B) hold:

$$EIy''_{OB}(s)=-\frac{\sqrt{6}}{3}P_B(s-L) \tag{13A}$$

where E is the Yong's modulus of the beam, $I = \frac{\pi}{64} d^4$ is the quadratic moment of the section.

And two successive integrations of the above equation give:

$$EIy'_{OB}(s) = -\frac{\sqrt{6}}{6} P_B (s-L)^2 + C_B \tag{13B}$$

and

$$EIy_{OB}(s) = -\frac{\sqrt{6}}{18} P_B (s-L)^3 + C_B s + D_B \tag{13C}$$

As point B is free, there is only one displacement boundary condition for beam OB:

$$y_{OB}(0) = 0 \tag{B1-2}$$

By using the above boundary condition in Eq. (13C), the coefficient D_B can be found and the equation can be then rewritten as follows:

$$EIy_{OB}(s) = -\frac{\sqrt{6}}{18} P_B \left[(s-L)^3 + L^3 \right] + C_B s \tag{14}$$

As the rotation of beam OA and OB at the point O is equal due to their rigid-rigid connection, that is $y'_{OA}(0)\vec{t}_{A2} = y'_{OB}(0)\vec{t}_{B2}$, and $\vec{t}_{A2} = -\vec{t}_{B2}$ as shown in Eq. (6), the following displacement (rotation) compatibility holds:

$$y'_{OA}(0) + y'_{OB}(0) = 0 \tag{B1-3}$$

By substituting Eqs. (11B_1) and (13B_1) into Eq. (B1-3), the following is obtained:

$$C_B = \sqrt{2} M_{Ax} L + \frac{\sqrt{6}}{6} (P_A + P_B - H) L^2 \tag{15}$$

By neglecting the shearing effect of the beams, the global displacement at the points A and B from point O due to the bending and compression are expressed as follow:

$$\vec{u}_A = y_{OA}(L)\vec{t}_{A1} + \frac{L}{ES}(\vec{P}_A \cdot \vec{n}_A)\vec{n}_A \tag{16A}$$

$$\vec{u}_B = y_{OB}(L)\vec{t}_{B1} + \frac{L}{ES}(\vec{P}_B \cdot \vec{n}_B)\vec{n}_B \tag{16B}$$

Substituting Eqs. (4), (6), (8A), (11C), (14) and (15) into Eqs. (16A) and (16B), these last two Eqs. can be rewritten as follows

$$\vec{u}_A = \frac{L^2}{EI}\left[-\frac{\sqrt{3}}{6} M_{Ax} - \frac{1}{18}(P_A - H)L \right] \begin{Bmatrix} -1 \\ -1 \\ -2 \end{Bmatrix} + \frac{(-P_A - 2H)L}{3ES} \begin{Bmatrix} -1 \\ -1 \\ 1 \end{Bmatrix} \tag{17A}$$

$$\vec{u}_B = \frac{L^2}{EI}\left[\frac{\sqrt{3}}{3} M_{Ax} + \frac{1}{18}(3P_A + 2P_B - 3H)L \right] \begin{Bmatrix} 1 \\ 1 \\ -2 \end{Bmatrix} - \frac{P_B L}{3ES} \begin{Bmatrix} 1 \\ 1 \\ 1 \end{Bmatrix} \tag{17B}$$

For beam *OA* and *OB* the following displacement compatibility holds:

$$W_A = W_B \tag{B1-4}$$

By using the above equation and the values in Eq. (17A) and (17B), the following is obtained:

$$9\sqrt{3}M_{Ax} + 2\left(2P_A + P_B - 2H\right)L - 3\left(P_A - P_B + 2H\right)\frac{I}{SL} = 0 \tag{A-2}$$

By using moment equilibrium for beam *OC* and the modeling in Fig. 3.A, the moment on the section is found in three dimensions:

$$\vec{M}_{OC}(s) = \vec{M}_C + (L-s)\vec{n}_C \wedge \vec{P}_C = M_{OCxl}\vec{n}_C + M_{OCyl}\vec{t}_{C1} + M_{OCzl}\vec{t}_{C2} \tag{18}$$

with

$$M_{OCxl} = -\frac{\sqrt{3}}{3}\left(M_{Cx} - M_{Cy} + M_{Cz}\right);$$

$$M_{OCyl} = \frac{\sqrt{2}}{2}H(s-L) + \frac{\sqrt{6}}{6}\left(M_{Cx} - M_{Cy} - 2M_{Cz}\right);$$

$$M_{OCzl} = \frac{\sqrt{6}}{6}\left(P_A + H + P_B\right)(s-L) - \frac{\sqrt{2}}{2}\left(M_{Cx} + M_{Cy}\right)$$

And by using the same method for beam *OD*, and keeping the component expressions of $\vec{M}_{OC}(s)$, the following is obtained:

$$\vec{M}_{OD}(s) = \vec{M}_D + (L-s)\vec{n}_D \wedge \vec{P}_D = -M_{OCxl}\vec{n}_D - M_{OCyl}\vec{t}_{D1} + M_{OCzl}\vec{t}_{D2} \tag{19}$$

By using Eq. (16) for beam *OC*, the displacement $y_{OC}(s)$ in the $\vec{t}_{C1}$ direction and the moment in the $\vec{t}_{C2}$ direction give:

$$EIy''_{OC}(s) = M_{OCzl} = -\frac{\sqrt{2}}{2}\left(M_{Cx} + M_{Cy}\right) + \frac{\sqrt{6}}{6}\left(P_A + H + P_B\right)(s-L) \tag{20A}$$

Two successive integrations of the above equation will give:

$$EIy'_{OC}(s) = -\frac{\sqrt{2}}{2}\left(M_{Cx} + M_{Cy}\right)s + \frac{\sqrt{6}}{12}\left(P_A + H + P_B\right)(s-L)^2 + C_{Cy} \tag{20B}$$

and

$$EIy_{OC}(s) = -\frac{\sqrt{2}}{4}\left(M_{Cx} + M_{Cy}\right)s^2 + \frac{\sqrt{6}}{36}\left(P_A + H + P_B\right)(s-L)^3 + C_{Cy}s + D_{Cy} \tag{20C}$$

By using the displacement boundary conditions in Table 1, and the assumption that point *O* is fixed in the local system, the following boundary conditions hold：

$$y_{OC}(0) = y'_{OC}(L) = 0 \tag{B1-5}$$

By substituting the above boundary conditions into Eqs. (20B) and (20C) respectively, the unknown coefficients C_{Cy} and D_{Cy} can be found and then these two Eqs. become:

$$EIy'_{OC}(s) = -\frac{\sqrt{2}}{2}\left(M_{Cx}+M_{Cy}\right)(s-L)+\frac{\sqrt{6}}{12}\left(P_A+H+P_B\right)(s-L)^2 \tag{20B_1}$$

$$EIy_{OC}(s) = -\frac{\sqrt{2}}{4}\left(M_{Cx}+M_{Cy}\right)s(s-2L)+\frac{\sqrt{6}}{36}\left(P_A+H+P_B\right)\left[(s-L)^3+L^3\right] \tag{20C_1}$$

By using Eq. (18), the displacement $-z_{OC}(s)$ in the $\vec{t}_{C2}$ direction and the moment in the $\vec{t}_{C1}$ direction give:

$$-EIz''_{OC}(s) = M_{OCyl} = \frac{\sqrt{6}}{6}\left(M_{Cx}-M_{Cy}-2M_{Cz}\right)+\frac{\sqrt{2}}{2}H(s-L) \tag{21A}$$

And then two successive integrations of the above equation give:

$$-EIz'_{OC}(s) = \frac{\sqrt{6}}{6}\left(M_{Cx}-M_{Cy}-2M_{Cz}\right)s+\frac{\sqrt{2}}{4}H(s-L)^2+C_{Cz} \tag{21B}$$

and

$$-EIz_{OC}(s) = \frac{\sqrt{6}}{12}\left(M_{Cx}-M_{Cy}-2M_{Cz}\right)s^2+\frac{\sqrt{2}}{12}H(s-L)^3+C_{Cz}s+D_{Cz} \tag{21C}$$

By using the boundary conditions in Table 1 and the assumption that point *O* has no displacement in its local coordinate system, the following two boundary conditions hold：

$$z_{OC}(0) = z'_{OC}(L) = 0 \tag{B1-6}$$

By substituting the above boundary conditions into Eqs. (21B) and (21C), the unknown coefficients C_{Cz} and D_{Cz} can be found and these two equations become:

$$-EIz'_{OC}(s) = \frac{\sqrt{6}}{6}\left(M_{Cx}-M_{Cy}-2M_{Cz}\right)(s-L)+\frac{\sqrt{2}}{4}H(s-L)^2 \tag{21B_1}$$

$$-EIz_{OC}(s) = \frac{\sqrt{6}}{12}\left(M_{Cx}-M_{Cy}-2M_{Cz}\right)s(s-2L)+\frac{\sqrt{2}}{12}H\left[(s-L)^3+L^3\right] \tag{21C_1}$$

For beam *OD*, in comparing the moment's components in Eqs. (18) and (19), the beams' displacements in the $\vec{t}_{D2}$ and $\vec{t}_{D1}$ directions due to the bending moments in the $\vec{t}_{D1}$ and $\vec{t}_{D2}$ directions, respectively hold:

$$\begin{cases} y_{OD}(s) = y_{OC}(s) \\ z_{OD}(s) = -z_{OC}(s) \end{cases} \tag{22A}$$

and

$$\begin{cases} y'_{OD}(s) = y'_{OC}(s) \\ z'_{OD}(s) = -z'_{OC}(s) \end{cases} \tag{22B}$$

The torsion angle α_{OC} at point *C* from point *O* due to the torsion moment M_{OCxl} in Eq. (18) can be determined as follows：

$$\alpha_{OC} = M_{OCxl}\frac{L}{GI_O} = (1+\nu)M_{OCxl}\frac{L}{EI} = -\alpha_{CO} \tag{23}$$

By using Eq. (19), the torsion angle at point *D* from point *O* can be expressed as follows:

$$\alpha_{OD} = -\alpha_{OC} \tag{24}$$

By using Eqs. (4), (6), (20B_1), (21B_1) and (23), the global rotation angle vector at point *O* of beam *OC* can be expressed as:

$$\vec{\theta}_{OC}(0) = -z'_{OC}(0)\vec{t}_{C1} + y'_{OC}(0)\vec{t}_{C2} + \alpha_{CO}\vec{n}_C = \theta_{OCx}(0)\vec{i} + \theta_{OCy}(0)\vec{j} + \theta_{OCz}(0)\vec{k} \tag{25}$$

With

$$\begin{cases} \theta_{OCx}(0) = \dfrac{L}{3EI}\left(-\left(2M_{Cx} + M_{Cy} - M_{Cz}\right) - (1+\nu)\left(M_{Cx} - M_{Cy} + M_{Cz}\right) - \dfrac{\sqrt{3}}{4}\left(P_A + P_B\right)L\right) \\ \theta_{OCy}(0) = \dfrac{L}{3EI}\left(-\left(M_{Cx} + 2M_{Cy} + M_{Cz}\right) + (1+\nu)\left(M_{Cx} - M_{Cy} + M_{Cz}\right) - \dfrac{\sqrt{3}}{4}\left(P_A + 2H + P_B\right)L\right) \\ \theta_{OCz}(0) = \dfrac{L}{3EI}\left(\left(M_{Cx} - M_{Cy} - 2M_{Cz}\right) - (1+\nu)\left(M_{Cx} - M_{Cy} + M_{Cz}\right) - \dfrac{\sqrt{3}}{2}HL\right) \end{cases}$$

With the same method for beam *OD* and by using Eqs. (4), (6), (20B_1), (21B_1), (22B), (23) and (24), and compared to Eq. (25), the global rotation angle vector at point *O* of beam *OD* can be expressed as:

$$\vec{\theta}_{OD}(0) = -z'_{OD}(0)\vec{t}_{D1} + y'_{OD}(0)\vec{t}_{D2} + \alpha_{DO}\vec{n}_D = -\theta_{OCy}(0)\vec{i} - \theta_{OCx}(0)\vec{j} - \theta_{OCz}(0)\vec{k} \tag{26}$$

And beam *OC* and *OD* have the same global rotation vector at point *O*:

$$\vec{\theta}_{OC}(0) = \vec{\theta}_{OD}(0) \tag{B1-7}$$

As the points *C* and *D* are symmetric with respect to the plane *X*=*Y*, by using the above boundary condition in Eqs. (25) and (26) and, the following two conditions hold:

$$\theta_{OCx}(0) + \theta_{OCy}(0) = 0 \tag{B1-7A}$$

$$\theta_{OCz}(0) = 0 \tag{B1-7B}$$

By using Eq. (25) in Eqs. (B1-7A) and (B1-7B) respectively, the following holds:

$$2\sqrt{3}\left(M_{Cx} + M_{Cy}\right) + \left(P_A + H + P_B\right)L = 0 \tag{A-3}$$

$$2\left(M_{Cx} - M_{Cy} - 2M_{Cz}\right) - 2(1+\nu)\left(M_{Cx} - M_{Cy} + M_{Cz}\right) - \sqrt{3}HL = 0 \tag{A-4}$$

By considering the bending, compression but neglecting the shearing effect, and using Eqs. (4), (6), (8B) , (21C_1) and (22A), the global displacement of point *C* from point *O* is obtained:

$$\vec{u}_C = z_{OC}(L)\vec{t}_{C2} + y_{OC}(L)\vec{t}_{C1} + \frac{L}{ES}\left(\vec{P}_C \cdot \vec{n}_C\right)\vec{n}_C$$

$$= -\frac{1}{EI}\left(-\frac{\sqrt{3}}{12}\left(M_{Cx} - M_{Cy} - 2M_{Cz}\right)L^2 + \frac{1}{12}HL^3\right)\begin{Bmatrix}-1\\-1\\0\end{Bmatrix} \tag{27}$$

$$+\frac{1}{EI}\left(\frac{\sqrt{3}}{12}\left(M_{Cx} + M_{Cy}\right)L^2 + \frac{P_A + H + P_B}{36}L^3\right)\begin{Bmatrix}1\\-1\\-2\end{Bmatrix} - \frac{L}{ES}\frac{P_A - 2H + P_B}{6}\begin{Bmatrix}-1\\1\\-1\end{Bmatrix}$$

As point *C* is on the symmetric plane *X*=0, therefore,

$$U_A = U_C \tag{B1-8}$$

And the imposed displacement in the *Z*-direction at point *A* holds:

$$W_A = W_A - W_C = W \tag{B1-9}$$

By using the displacement boundary condition Eq. (B1-8) in Eqs. (17A) and (27), the following is obtained:

$$-6\sqrt{3}\left(M_{Ax} - M_{Cy} - M_{Cz}\right) + \left(-P_A + P_B + 6H\right)L + 6\left(-P_A + P_B - 6H\right)\frac{I}{SL} = 0 \tag{A-5}$$

By using Eqs. (B1-9) in Eqs. (17A) and (27), the following is obtained:

$$3\sqrt{3}\left(2M_{Ax} + M_{Cx} + M_{Cy}\right) + \left(3P_A - H + P_B\right)L - 3\left(3P_A + 2H + P_B\right)L\frac{I}{SL^2} = 18\frac{W}{L^2} \tag{A-6}$$

Another computability condition is:

$$\vec{\theta}_{OC}(0) = \vec{\theta}_{OA}(0) \tag{B1-10}$$

In which three dimensions will be satisfied, respectively as follow:

$$\theta_{OCx}(0) = \theta_{OAx}(0);\ \theta_{OCy}(0) = \theta_{OAy}(0);\ \theta_{OCz}(0) = \theta_{OAz}(0)$$

It is noted that $\theta_{OAz}(0) = 0$, therefore $\theta_{OCz}(0) = 0$, which is already used in Eq. (B1-7B).

As indicated in Eq. (B1-7A) $\theta_{OCx}(0) + \theta_{OCy}(0) = 0$, and point *A* is on the symmetric plane $\theta_{OAx}(0) + \theta_{OAy}(0) = 0$, therefore, $\theta_{OCx}(0) = \theta_{OAx}(0)$ or $\theta_{OCy}(0) = \theta_{OAy}(0)$ are linear related. Anyone of them can be chosen as the boundary condition.

By using the condition $\theta_{OCx}(0) = \theta_{OAx}(0)$ in Eq. (B1-10), Eq. (12) and Eq. (25):

$$\left(-3M_{Ax} + 2M_{Cx} + M_{Cy} - M_{Cz}\right) + \left(1+\nu\right)\left(M_{Cx} - M_{Cy} + M_{Cz}\right) + \frac{\sqrt{3}}{4}\left(-P_A + P_B + 2H\right)L = 0 \tag{A-7}$$

Eqs. (A-1) to (A-7) form a system of linear equations with the 7 unknown variables P_A, P_B, H, M_{Ax}, M_{Cx}, M_{Cy}, and M_{Cz}, thus P_A+P_B is a function of *W* and it can be found by solving these equations. And the effective elastic modulus can be obtained as follows:

$$\frac{E_{eff}}{E} = -\frac{2\left(P_A + P_B\right)}{EbW}$$
$$= 6\frac{\left(1440\nu + 2592\right)\phi^2 + \left(5844\nu + 6804\right)\phi + \left(385\nu + 441\right)}{\left(8640\nu + 15552\right)\phi^3 + \left(38232\nu + 46008\right)\phi^2 + \left(10890\nu + 12582\right)\phi + \left(496\nu + 567\right)}\beta\rho^2 \quad (28)$$

with $\beta = \frac{\sqrt{3}}{18\pi}$; $\rho = \frac{2\sqrt{3}\pi d^2}{b^2}$ and $\phi = \beta\rho$.

ρ is the density of the structure. Only when ρ is very small, the relative effective elastic modulus can be approximated as ρ^2.

2) ***Modeling for upper bound of effective elastic modulus***

The upper bound of effective elastic modulus in the *Z*-direction is obtained by imposing $m \to \infty$ and $n \to \infty$. The forces, moments and boundary conditions will be imposed in 1/8 cell to replace $m \to \infty$ and $n \to \infty$. The boundary conditions with constant displacement in the global coordinate system are given in Table 2:

point *A*	$U_A = V_A = 0;\ w_A = W;\ \theta_{Ax} = \theta_{Ay} = \theta_{Az} = 0$	point *B*	$W_B = W;\ \theta_{Bx} = \theta_{By} = \theta_{Bz} = 0$
point *C*	$U_C = W_C = 0;\ \theta_{Cx} = \theta_{Cy} = \theta_{Cz} = 0$	point *D*	$V_D = W_D = 0;\ \theta_{Dx} = \theta_{Dy} = \theta_{Dz} = 0$

Table 2 Constant displacement boundary conditions for ∞×∞ cells structure

By considering the double symmetry of the unit cell, and four beams shear point *O* as origin with the rigid-rigid connection one another, the complementary boundary conditions with non-constant displacement are:

$$U_B = U_D;\ V_B = V_C$$

$$\vec{\theta}_{OA}(0) = \vec{\theta}_{OB}(0) = \vec{\theta}_{OC}(0) = \vec{\theta}_{OD}(0)$$

For the forces, because of the double symmetry in the plane *OXY* and two pairs of parallel mirrors in the *X*-direction *and* the *Y*-direction respectively, the points *A* and *B* have the same solicitation *P* in the *Z*-direction, and the points *C* and *D* have the same resultant *P* in the *Z*-direction. Therefore,

$$\vec{P}_A = \vec{P}_B = -P\vec{k};\ \vec{P}_C = \vec{P}_D = P\vec{k} \quad (29)$$

As there are no forces in the plane *xOy*, the moment in the *Z*-direction doesn't exist at the points *A*, *B*, *C* and *D*. Taking into consideration double symmetry in the plane XO_gY, the moments at the points as shown in Fig. 3.B are supposed as follows:

$$\vec{M}_A = \begin{Bmatrix} M \\ -M \end{Bmatrix},\ \vec{M}_B = \begin{Bmatrix} -M \\ M \end{Bmatrix},\ \vec{M}_C = \begin{Bmatrix} M \\ M \end{Bmatrix},\ \vec{M}_D = \begin{Bmatrix} -M \\ -M \end{Bmatrix} \quad (30)$$

The force and moment equilibrium Eqs. (7A) and (7B) are verified by Eqs. (29) and (30).

The moments on the section of beam *OA* and *OB* can be found as follow:

$$\vec{M}_{OA}(s) = \vec{M}_A + \vec{n}_A\left(L - s\right) \times \vec{P}_A = M_{OA}\vec{t}_{A2} \quad (31A)$$

with $M_{OA} = -\frac{\sqrt{6}}{3}P\left(s - L\right) + \sqrt{2}M$, and

$$\vec{M}_{OB}(s)=\vec{M}_B+\vec{n}_B(L-s)\times\vec{P}_B=M_{OA}\vec{t}_{B2} \tag{31B}$$

Furthermore, the moments on the section of beam *OC* and *OD* can be found as follow:

$$\vec{M}_{OC}(s)=\vec{M}_C+(L-s)\vec{n}_C\wedge\vec{P}_C=-M_{OA}\vec{t}_{C2} \tag{31C}$$

and

$$\vec{M}_{OD}(s)=\vec{M}_D+(L-s)\vec{n}_D\wedge\vec{P}_D=-M_{OA}\vec{t}_{D2} \tag{31D}$$

In Eqs. (31A) to (31D), the four beams have the same bending deformation determined by M_{OA}. By using (31A) for beam *OA*, the displacement $y_{OA}(s)$ in the $\vec{t}_{A1}$ direction and the moment in the $\vec{t}_{A2}$ direction hold:

$$EIy''_{OA}(s)=M_{OA}=-\frac{\sqrt{6}}{3}P(s-L)+\sqrt{2}M \tag{32A}$$

And two successive integrations give:

$$EIy'_{OA}(s)=-\frac{\sqrt{6}}{6}P(s-L)^2+\sqrt{2}Ms+C_{Ay} \tag{32B}$$

$$EIy_{OA}(s)=-\frac{\sqrt{6}}{18}P(s-L)^3+\frac{\sqrt{2}}{2}Ms^2+C_{Ay}s+D_{Ay} \tag{32C}$$

It is supposed in their local coordinate system the beam *OA* has no displacement at point *O* and it has no rotation at point *A*. The displacement boundary conditions are as follows:

$$y_{OA}(0)=y'_{OA}(L)=0 \tag{B2-1}$$

By using the above boundary conditions in Eqs. (32B) and (32C), they become:

$$EIy'_{OA}(s)=-\frac{\sqrt{6}}{6}P(s-L)^2+\sqrt{2}M(s-L) \tag{33A}$$

$$EIy_{OA}(s)=-\frac{\sqrt{6}}{18}P\left[(s-L)^3+L^3\right]+\frac{\sqrt{2}}{2}Ms(s-2L) \tag{33B}$$

As beam *OB* has the same moment expression in $\vec{t}_{B2}$ as that of beam *OA* in the $\vec{t}_{A2}$ direction, the following holds:

$$y'_{OB}(s)=y'_{OA}(s) \tag{34A}$$

and

$$y_{OB}(s)=y_{OA}(s) \tag{34B}$$

By neglecting the shear effect of the beams, the global displacement at point *A* due to the bending and compression is expressed as:

$$\vec{u}_A=y_{OA}(L)\vec{t}_{A1}+\frac{L}{ES}(\vec{P}_A\cdot\vec{n}_A)\vec{n}_A \tag{35}$$

By using Eqs. (4), (6), (29) and (33B) in Eq. (35), Eq. (35) is expressed numerically:

$$\vec{u}_A = \frac{1}{EI}\left(-\frac{\sqrt{2}}{2}ML^2 - \frac{\sqrt{6}}{18}PL^3\right)\frac{1}{\sqrt{6}}\begin{Bmatrix}-1\\-1\\-2\end{Bmatrix} + \frac{-PL}{\sqrt{3}ES}\frac{1}{\sqrt{3}}\begin{Bmatrix}-1\\-1\\1\end{Bmatrix} \tag{36}$$

As the rotation angle vector of beam *OA* and *OB* at point *O* is equal due to the rigid-rigid connection,

$$y'_{OA}(0)\vec{t}_{A2} = y'_{OB}(0)\vec{t}_{B2} \tag{37}$$

and as $\vec{t}_{A2} = -\vec{t}_{B2}$ indicated in Eq. (6), and $y'_{OB}(s) = y'_{OA}(s)$ indicated in Eq. (34A), the following holds by using the above equation:

$$y'_{OA}(0) = 0 \tag{B2-2}$$

By using Eqs. (33A) and (B2-2), the following equation holds:

$$6M + \sqrt{3}PL = 0 \tag{B-1}$$

As beam *OC* has the same moment expression in $-\vec{t}_{C2}$ as that of beam *OA* in the $\vec{t}_{A2}$ direction, the following holds:

$$y_{OC}(s) = -y_{OA}(s) \tag{38}$$

Therefore, by using Eq. (33B) and (38) the following holds:

$$EIy_{OC}(s) = -EIy_{OA}(s) = \frac{\sqrt{6}}{18}P\left[(s-L)^3 + L^3\right] - \frac{\sqrt{2}}{2}Ms(s-2L) \tag{39}$$

By neglecting the shear effect, the global displacement of point *C* due to the bending and compressing can be expressed by:

$$\vec{u}_C = y_{OC}(L)\vec{t}_{C1} + \frac{L}{ES}\left(\vec{P}_C \cdot \vec{n}_C\right)\vec{n}_C \tag{40A}$$

And numerically,

$$\vec{u}_C = \frac{1}{EI}\left(\frac{\sqrt{3}}{6}ML^2 + \frac{1}{18}PL^3\right)\begin{Bmatrix}1\\-1\\-2\end{Bmatrix} - \frac{1}{3}\frac{PL}{ES}\begin{Bmatrix}-1\\1\\-1\end{Bmatrix} \tag{40B}$$

The imposed displacement holds:

$$W_A - W_C = W, \tag{B2-3}$$

By using Eqs. (36), (40B) and (B2-3), the following is obtained:

$$6\sqrt{3}ML^2 + 2PL^3 - 6P\frac{IL}{S} = 9EIW \tag{B-2}$$

Eqs. (B-1) and (B-2) form a system of linear equations with M and P as unknown variables. And the effective elastic modulus in the Z-direction can be obtained and expressed as a function related to the density ρ of the structure by using Eqs. (1), (B-1) and (B-2):

$$\frac{E_{Eff}^{Upper}}{E} = -\frac{4}{b}\frac{P}{EW} = \frac{6\beta\rho^2}{1+6\beta\rho} \tag{41}$$

3) ***Modeling for structure with border constraint***

For the structure with border constraint, the boundary conditions with constant displacement in the global coordinate system are in Table 3:

point A	$U_A = V_A = 0;\ W_A = W;\ \theta_{Ax} = \theta_{Ay} = \theta_{Az} = 0$	point B	$U_B = V_B = 0; W_B = W;\ \theta_{Bx} = \theta_{By} = \theta_{Bz} = 0$
point C	$U_C = V_C = W_C = 0;\ \theta_{Cx} = \theta_{Cy} = \theta_{Cz} = 0$	point D	$U_D = V_D = W_D = 0;\ \theta_{Dx} = \theta_{Dy} = \theta_{Dz} = 0$

Table 3 Constant displacement boundary conditions for structure with border constraint

As in other cases, the complementary boundary conditions with non-constant displacement are:

$$\vec{\theta}_{OA}(0) = \vec{\theta}_{OB}(0) = \vec{\theta}_{OC}(0) = \vec{\theta}_{OD}(0)$$

For the forces due to the double symmetry of the unit cell in the plane OXY and two pairs of parallel rigid panels at the borders in the X-direction and the Y-direction respectively, the points A and B have the same solicitation P in the Z-direction, and the points C and D have the same resultant P in the Z-direction. Therefore the force solicitations and reaction are supposed to be as follows in satisfying Eq. (7A):

$$\vec{P}_A = \begin{Bmatrix} H \\ H \\ -P \end{Bmatrix};\ \vec{P}_B = \begin{Bmatrix} -H \\ -H \\ -P \end{Bmatrix};\ \vec{P}_C = \begin{Bmatrix} H \\ -H \\ P \end{Bmatrix};\ \vec{P}_D = \begin{Bmatrix} -H \\ H \\ P \end{Bmatrix}; \tag{42}$$

As there are no forces in the plane Oxy, the moment in the Z-direction doesn't exist at the points A, B, C and D. Taking into consideration of double symmetry in the plane XOY, the moments at the points as shown in Fig. 3.C are supposed as follows:

$$\vec{M}_A = \begin{Bmatrix} M \\ -M \end{Bmatrix},\ \vec{M}_B = \begin{Bmatrix} -M \\ M \end{Bmatrix},\ \vec{M}_C = \begin{Bmatrix} M \\ M \end{Bmatrix},\ \vec{M}_D = \begin{Bmatrix} -M \\ -M \end{Bmatrix} \tag{43}$$

The moment equilibrium Eq. (7B) is also verified by Eq. (43).

The moments on the section of beam OA and OB can be found as follow:

$$\vec{M}_{OA}(s) = \vec{M}_A + (L-s)\vec{n}_A \times \vec{P}_A = \sqrt{2}\left[M - (s-L)\frac{\sqrt{3}}{3}(P-H)\right]\vec{t}_{A2} \tag{44A}$$

and

$$\vec{M}_{OB}(s) = \vec{M}_B + \vec{n}_B(L-s) \times \vec{P}_B = \sqrt{2}\left[M - (s-L)\frac{\sqrt{3}}{3}(P-H)\right]\vec{t}_{B2} \tag{44B}$$

For beam OA, the displacement $y_{OA}(s)$ in the $\vec{t}_{A1}$ direction and the moment in the $\vec{t}_{A2}$ direction have:

$$EIy''_{OA}(s) = -\frac{\sqrt{6}}{3}(P-H)(s-L) + \sqrt{2}M \tag{45A}$$

And two successive integrations give:

$$EIy'_{OA}(s) = -\frac{\sqrt{6}}{6}(P-H)(s-L)^2 + \sqrt{2}Ms + C_{Ay} \tag{45B}$$

$$EIy_{OA}(s) = -\frac{\sqrt{6}}{18}(P-H)(s-L)^3 + \frac{\sqrt{2}}{2}Ms^2 + C_{Ay}s + D_{Ay} \tag{45C}$$

It is supposed in their local coordinate system the beam *OA* has no displacement at point *O* and it has no rotation at point *A*. The displacement boundary conditions are as follows:

$$y_{OA}(0) = y'_{OA}(0) = y'_{OA}(L) = 0 \tag{B3-1}$$

By using the above boundary conditions in Eqs. (39B) and (39C), the following are obtained:

$$EIy'_{OA}(s) = -\frac{\sqrt{6}}{6}(P-H)(s-L)^2 + \sqrt{2}M(s-L) \tag{46A}$$

$$EIy_{OA}(s) = -\frac{\sqrt{6}}{18}(P-H)\left[(s-L)^3 + L^3\right] + \frac{\sqrt{2}}{2}Ms(s-2L) \tag{46B}$$

and

$$6M + \sqrt{3}(P-H)L = 0 \tag{C-1}$$

The global displacement of point *A* shares the same expression in Eq. (35). Thus by using Eqs. (4), (6), (42) and (46B) in Eq. (35), Eq. (35) is expressed numerically as follows:

$$\vec{u}_A = \frac{1}{EI}\left[-\frac{\sqrt{2}}{2}ML^2 - \frac{\sqrt{6}}{18}(P-H)L^3\right]\frac{1}{\sqrt{6}}\begin{Bmatrix}-1\\-1\\-2\end{Bmatrix} + \frac{-(P+2H)L}{3ES}\begin{Bmatrix}-1\\-1\\1\end{Bmatrix} \tag{47}$$

The moment in the section of beam *OC* are found to be:

$$\vec{M}_{OC}(s) = \vec{M}_C + (L-s)\vec{n}_C \times \vec{P}_C = \sqrt{2}\left[-M + \frac{\sqrt{3}}{3}(P-H)(s-L)\right]\vec{t}_{C2} \tag{48}$$

$$EIy_{OC}(s) = -\frac{\sqrt{2}}{2}Ms(s-2L) + \frac{\sqrt{6}}{18}(P-H)\left[(s-L)^3 + L^3\right] \tag{49}$$

By neglecting the shear effect, the global displacement of point *C* due to the bending and compressing can be expressed by:

$$\vec{u}_C = y_{OC}(L)\vec{t}_{C1} + \frac{L}{ES}\left(\vec{P}_C \cdot \vec{n}_C\right)\vec{n}_C \tag{50}$$

By using Eqs. (4), (6), (42) and (49) in Eq. (50), Eq. (50) is expressed numerically as follows:

$$\vec{u}_C = \frac{1}{EI}\left(\frac{\sqrt{2}}{2}ML^2 + \frac{\sqrt{6}}{18}(P-H)L^3\right)\frac{1}{\sqrt{6}}\begin{Bmatrix}1\\-1\\-2\end{Bmatrix} - \frac{L}{ES}(P+2H)\frac{1}{3}\begin{Bmatrix}-1\\1\\-1\end{Bmatrix} \tag{51}$$

The imposed displacement in the *Z*-direction holds:

$$W_A - W_C = W \tag{B3-2}$$

And as point *C* is on the symmetric plane *X*=0, the following holds:

$$V_C = 0 \tag{B3-3}$$

By using Eqs. (B3-2), (47) and (51), the following is obtained:

$$6\sqrt{3}M + 2(P-H)L - 6(P+2H)\frac{I}{SL^2} = 9EW\frac{I}{L^2} \tag{C-2}$$

By using Eqs. (B3-3) and (51), the following is obtained:

$$3\sqrt{3}M + (P-H)L + 6\frac{I}{SL}(P+2H) = 0 \tag{C-3}$$

By using Eqs. (C-1), (C-2) and (C-3), the effective elastic modulus in the *Z*-direction can be obtained and expressed related to the density ρ of the structure:

$$\frac{E_{Eff}^{Upper}}{E} = -\frac{4P}{EbW} = \frac{1}{9}(1+24\beta\rho)\rho \tag{52}$$

2.4 Finite element modeling by using beam theory

The finite element method taking into consideration the tension/compression, bending and torsion without shearing effect has been used. Therefore the stiffness matrix contains three kinds of stiffness: tension/compression, bending and torsion. A beam consisting of point *i* and *j* has 12 general displacement variables $u_i, v_i, w_i, \theta_{ix}, \theta_{iy}, \theta_{iz}, u_j, v_j, w_j, \theta_{jx}, \theta_{jy}, \theta_{jz}$ accordingly in the beam (local) coordinate system.

1) Stiffness matrix of a beam in the local coordinate system [24]

For the uniaxial tension or compression of a beam, by using $f = Ku$, the unidimensional stiffness is:

$$K = \frac{ES}{L} \tag{53}$$

For homogenous bending, that is $I = I_y = I_z = I_O/2$, by using the bending theory of a beam element shown in Eqs. (A1) – (A7) in the annex, the stiffness matrix for bending around the *Z*-direction is:

$$[Z] = \begin{bmatrix} Z_{11} & Z_{12} & Z_{13} & Z_{14} \\ Z_{21} & Z_{22} & Z_{23} & Z_{24} \\ Z_{31} & Z_{32} & Z_{33} & Z_{34} \\ Z_{41} & Z_{42} & Z_{43} & Z_{44} \end{bmatrix} = \frac{EI}{L^3}\begin{bmatrix} 12 & 6L & -12 & 6L \\ 6L & 4L^2 & -6L & 2L^2 \\ -12 & -6L & 12 & -6L \\ 6L & 2L^2 & -6L & 4L^2 \end{bmatrix} \tag{54}$$

The bending deformation around the *Y*-direction is from *x* to z, the rotation is clockwise. By considering the rotation direction and by using the expressions in the stiffness matrix $[Z]$, the stiffness matrix for bending around the *Y*-direction can be expressed as:

$$[Y]=\begin{bmatrix} Z_{11} & -Z_{12} & Z_{13} & -Z_{14} \\ -Z_{21} & Z_{22} & -Z_{23} & Z_{24} \\ Z_{31} & -Z_{32} & Z_{33} & -Z_{34} \\ -Z_{41} & Z_{42} & -Z_{43} & Z_{44} \end{bmatrix} \tag{55}$$

For the torsion with $M=T\theta$, the unidimensional stiffness is:

$$T=GI_O/L \tag{56}$$

The global elemental element displacement-force matrix Eq. is therefore obtained from Eqs. (53-56) and has the expression as follows:

$$\begin{bmatrix} K & & & & & & -K & & & & & \\ & Z_{11} & & & & Z_{12} & & Z_{13} & & & & Z_{14} \\ & & Z_{11} & & -Z_{12} & & & & Z_{13} & & -Z_{14} & \\ & & & T & & & & & & -T & & \\ & & & & Z_{22} & & & & -Z_{23} & & Z_{24} & \\ & & & & & Z_{22} & & Z_{23} & & & & Z_{24} \\ & & & & & & K & & & & & \\ & & & & & & & Z_{33} & & & & Z_{34} \\ & & & sym & & & & & Z_{33} & & -Z_{34} & \\ & & & & & & & & & T & & \\ & & & & & & & & & & Z_{44} & \\ & & & & & & & & & & & Z_{44} \end{bmatrix} \begin{Bmatrix} u_i \\ v_i \\ w_i \\ \theta_{ix} \\ \theta_{iy} \\ \theta_{iz} \\ u_j \\ v_j \\ w_j \\ \theta_{jx} \\ \theta_{jy} \\ \theta_{jz} \end{Bmatrix} = \begin{Bmatrix} F_{ix} \\ F_{iy} \\ F_{iz} \\ M_{ix} \\ M_{iy} \\ M_{iz} \\ F_{jx} \\ F_{jy} \\ F_{jz} \\ M_{jx} \\ M_{jy} \\ M_{jz} \end{Bmatrix} \tag{57A}$$

The items in the cases that are not filled in the above matrix are zero. And the above matrix Eq. can be simplified as:

$$[K]_l\{u\}_l=\{f\}_l \tag{57B}$$

where $[K]_l$ is the global stiffness matrix, $\{u\}_l$ is the displacement vector and $\{f\}_l$ is the exterior force vector in the beam's local coordinate system.

2) Stiffness matrix of beam in the global coordinate system

For any vector the transformation matrix from the local coordinate system to the global one is composed of the directional vectors are $\vec{n}$, $\vec{t}_1$ and $\vec{t}_2$:

$$[R]=\begin{bmatrix} \vec{n} & \vec{t}_1 & \vec{t}_2 \end{bmatrix} \tag{58}$$

By considering one beam with two nodes, there are 12 degrees of freedom (DOF) considered as 4 vectors, thus the complete transformation matrix $[R_C]$ for the 12 DOF is then expressed as:

$$[R_C]_{12\times12} = \begin{bmatrix} R & 0 & 0 & 0 \\ 0 & R & 0 & 0 \\ 0 & 0 & R & 0 \\ 0 & 0 & 0 & R \end{bmatrix} \tag{59}$$

By using the transformation matrix in Eq. (59), as showed in Eq. (A8) in the annex, the global stiffness matrix is found as follows:

$$[K]_g = [R_C][K]_l[R_C]^T \tag{60}$$

In the elemental global stiffness matrix, the distribution of zero elements are in the following positions shown in Fig. 4 that can be served for the sparse matrix of the whole structure:

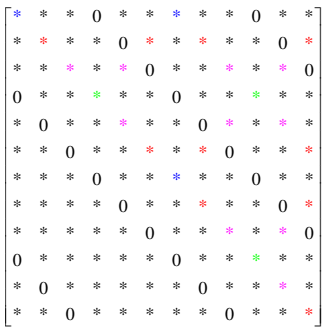

Fig. 4 Zero-value element positions in elemental matrix

3) Upper bounds of the effective elastic modulus E_{eff} of an $m\times n$ structure

In order to study the upper bounds of the effective elastic modulus that is a function of m and n for the $m\times n$ structure, without loss of generality, it is supposed that the number of rows m is constant, and the number of columns n varies from 1 to infinite. And each couple (m, n) gives an effective elastic modulus. The upper bound of the effective elastic modulus can be given by using the infinite number of cells ($n \to \infty$). And for the whole structure without fixing m, the upper bound can be found by using the infinite number of cells in rows and columns ($m \to \infty$; $n \to \infty$).

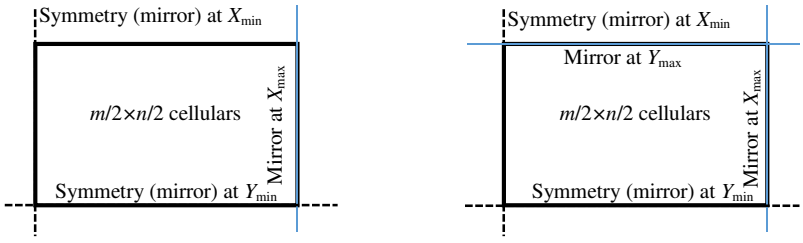

A) Infinite m B) Infinite m and infinite n

Fig. 5. Mirror settings for infinite numbers of cells

In the $m\times n$ structure, any two vertical parallel mirrors placed in the X- or the Y-direction will give an infinite number of cells in the direction that is perpendicular to the parallel mirrors. For example as shown in Fig. 5.A the symmetric plane (mirror) at X_{min} and the mirror at X_{max} will give an infinite number of cells in the X-direction and it doesn't depend on the values of n. That is, any value of n will give the same value of the effective elastic modulus. As shown in Fig. 5.B, two pairs of vertical mirrors in the X- and the Y-directions will give an infinite number of cells in both directions.

4) Boundary conditions for infinite n structure

In general, the choice of m or n is fixed is the same methodology. It is supposed that m is constant. For any constant m of $m \times n$ structure, $n \to \infty$ gives the upper bound of effective elastic stiffness. In finite element method, $n \to \infty$ is ensured by the boundary conditions by using a mirror at X_{max}. As any value of n with the mirror at X_{max}. gives the infinite assumption, n=1 is chosen.

For any point on the symmetrical plane (mirror) at X_{min}, the displacement boundary conditions are:

$$U_i = 0;\ \theta_{iy} = \theta_{iz} = 0 \tag{61}$$

As all the points on the mirror at X_{max} move conjointly in the X-direction, point i is chosen as the reference point, and the displacement boundary conditions for the points on this mirror are:

$$U_j = U_i \left(i \neq j\right);\ \theta_{jy} = \theta_{jz} = 0 \tag{62}$$

where the displacement u_i or the reference point is unknown. As the mirror at X_{max} is not a free border of the structure, a supplementary force equilibrium boundary condition will be used:

$$\sum F_{ix} = 0 \tag{63}$$

where i denotes all the nodes on the mirror at X_{max}.

For the boundary conditions for infinite m and infinite n structure, in addition to the boundary conditions in the X-direction, the boundary conditions in the Y-direction will be adopted by using the same method.

5) Stiffness matrix, displacement vector and force vector modification

The global stiffness matrix $\left[K\right]_g$ is singular. It becomes nonsingular by modifying it according to the boundary conditions. The global stiffness matrix and the displacement vector in the matrix Eq. $\left[K\right]_g \left\{U\right\} = \left\{F\right\}$ will be modified at the same time. This matrix Eq. is regarded as N_{equ} normal Eqs. where $N_{equ} \times N_{equ}$ is the dimension of the stiffness matrix. Initially, the force vector $\left\{F\right\}$ is set as $\vec{0}$ and the modification is executed in the following order:

a) For a constant displacement boundary condition $U_q = C$

This boundary condition concerns the points on the symmetric plane and the points on at Z_{max}. The coefficients in the q^{th} Eq. are rewritten:

$$K_{qr} = \begin{cases} 1\left(q = r\right) \\ 0\left(q \neq r\right) \end{cases} \tag{64A}$$

For the case $C \neq 0$, the following coefficients in the q^{th} Eq. are modified:

$$F_q = C \tag{64B}$$

In order to use the sparse matrix resolution method, more coefficients may be modified. Other directions denoted as r of the concerned points in which $K_{rq} \neq 0$ is used and F_q is modified as:

$$F_q \to F_q - \sum K_{rq} U_q \tag{64C}$$

and then K_{rq} is reset as zero.

$$K_{rq} = 0 \tag{64D}$$

b) For a conjoint movement boundary condition $U_j = U_i$

This boundary condition concerns the points on the mirror at $x_{\max}$. In this case $U_j - U_i$ is used as the new unknown variable at the place of U_j.

In the k^{th} equation ($k \neq j$), originally it is:

$$\sum_{A \neq i;\, A \neq j} K_{kA} U_A + K_{ki} U_i + K_{kj} U_j = F_k \tag{65}$$

In order to use $U_j - U_i$ as the new unknown variable the above equation is rewritten as follows:

$$\sum_{A \neq i;\, A \neq j} K_{kA} U_A + \left(K_{ki} + K_{kj}\right) U_i + K_{kj} \left(U_j - U_i\right) = F_k \tag{66}$$

For those Eqs. in which $K_{kj} \neq 0$, K_{ki} is rewritten as:

$$K_{ki} \rightarrow K_{ki} + K_{kj} \tag{67}$$

and in the j^{th} equation,

$$K_{jl} = \begin{cases} 1 \left(j = l\right) \\ 1 \left(j \neq l\right) \end{cases} \tag{68}$$

c) For the supplementary force equilibrium boundary condition

This boundary condition concerns the X-direction of all the points on the mirror at $X_{\max}$. In the i^{th} equation, the force equilibrium boundary condition in Eq. (63) is used. The X-direction of a concerned point is denoted as k, and the Y-direction of the concerned points is denoted as l, the coefficients K_{il} are modified as follows:

$$K_{il} \rightarrow \sum K_{kl} \tag{69}$$

After the resolution of the modified matrix equation, U_j is reset as U_i at the place of $U_j - U_i$.

2.5 Effective elastic modulus under compression with border constraint

As shown in Table 3, the problem of compression with border constraint has only constant displacement boundary condition. A normal solution of FE will give the effective elastic modulus under compression. The stiffness matrix is modified by using Eqs. (64A) to (64D) with the imposed constant displacement boundary conditions in order to dispose of its singularity.

3. Results and discussions

The sample of the rhombic dodecahedron structure in study has the following geometrical and mechanical parameter: b =5 mm; d =0.5 mm; $\nu = 0.3$. E =110 GPa. The porosity of this structure is 0.89. As the relative effective elastic modulus E_{eff}/E is independent of Young's modulus, Young's modulus E is not necessary to calculate the effective relative modulus. The relative effective elastic modulus in the Z-direction has been calculated by the FE method using beam theory neglecting shearing effect due to the capacity and efficiency of FE method. The upper and lower bounds given by analytical method are the same as those given by the FE method.

For the give geometrical parameters, the porosity of the structure remains the same independent of the number of cells. All the results in Fig. 6 are based on the same porosity.

Fig. 6.A, 6.B and 6.C show the individual relative effective elastic modulus E_{eff}/E for the structure with m=1, m=5 and m=40, and n varies from 1 to 40. For each case, the lower bound of E_{eff}/E is given by m×1 structure and the upper bound is given by m×∞ structure. All the curves start from the lower bound and tend to the upper bound. At the beginning, the curves increase rapidly, and then slows down. At the same time 99% and 98% of the upper bound are designed to indicate the range of application conditions. From these three Figures, it is observed that not all the values are in the range 98%-100% of the upper bound, especially for a small value of n, the value is far from the given range. In another way, the accurate homogenization of the structure is valid only for the structure with infinite number of cells, therefore it cannot be established based on a single cell. In practice, as infinite number of cells doesn't exist, an error range can be designed, such as 98% or other values according to the application request. And as m increases, the dimension of the structure increases, more values are out of the range 98%-100% of the upper bound. Therefore, the minimal value of m and n can be chosen as the reference m and the maximum as n to better predict the behavior in a designed range.

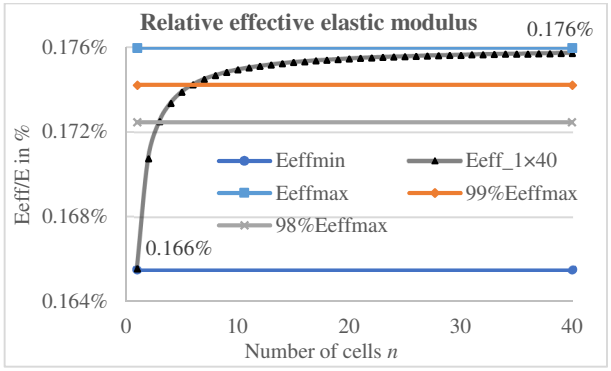

A) 1×40

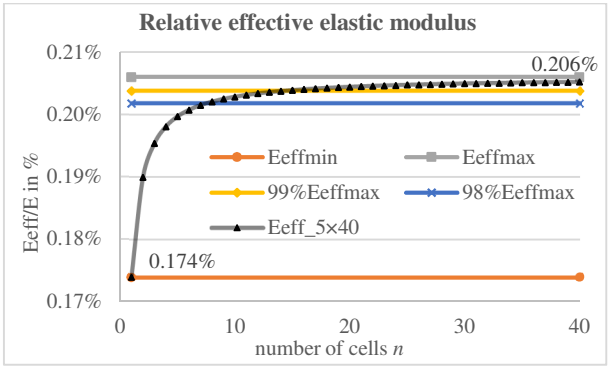

B) 5×40

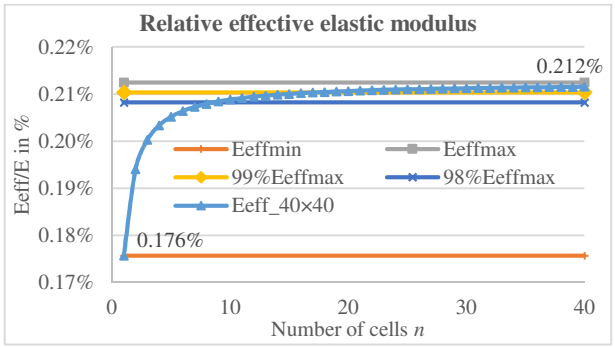

C) 40×40

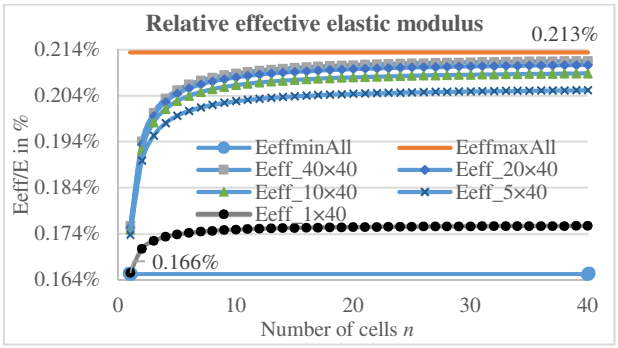

D) m×40

Fig. 6 Relative compressive effective elastic modulus without border constraint

Fig. 6.D shows the relative effective elastic modulus E_{eff}/E for the structure for different constant m from 1 to 40, and in each case n varies from 1 to 40. The global lower bound is given by 1×1 structure and the upper bound is given by ∞×∞ structure. As all the structures with different m and n have the same porosity, the relative effective elastic modulus E_{eff}/E cannot be expressed as a function purely related to the porosity, excepting for the global lower and upper bounds. The lower and upper bounds given by the FE method and analytical method are exactly the same.

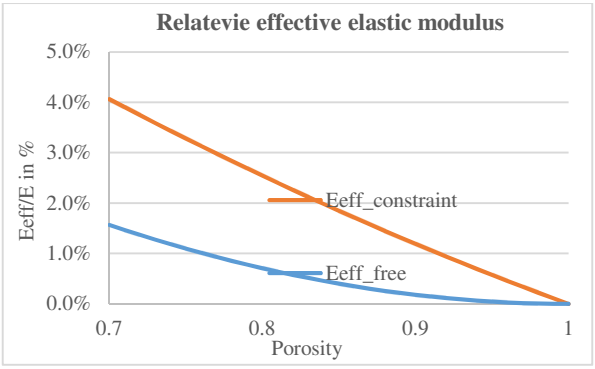

Fig. 7 Relative compressive effective elastic modulus with/without border constraint vs porosity

In Fig. 7, the upper bound of relative compressive effective elastic modulus without border constraint given by Eq. (41), and the relative compressive effective elastic modulus with border constraint given by Eq. (52) are presented. It is observed that these two curves tend to 0 when the porosity tends to 1. In practice, the value with border constraint is much higher than the upper bound without border constraint.

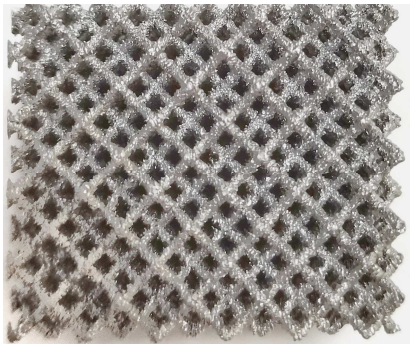

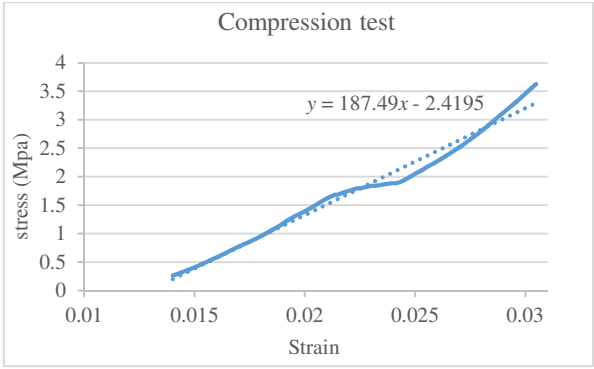

A) Fabricated Ti6Al4V structure of 4.75×4.75 cells B) Compression test of fabricated structure

Fig. 8 Experimental relative compressive effective elastic modulus

Fig. 8.A shows the parameters of experimental structure with 4.75×4.75 cells and height of 28.2mm. The specimen was manufactured using an Arcam A1 EBM system with a fine powder Ti6Al4V provided by Acram AB(Sweden). The average particle size of the powder was 76 μm. The specimen consists of a rhombic dodecahedral unit cell periodically arranged in three directions along the spatial coordinate axis and becomes a porous structure material with a cuboid frame. The relevant geometric parameters are the side length of the unit cell (b), the diameter of the struts (d), and the outer dimensions of the specimen. Table 4 shows the morphological characteristics and mechanical properties of the specimen. The compression test was carried out on a WGW-100H electronic universal testing machine with an initial strain rate of 0.001 mm/s at room temperature. The stress-strain relationship and elastic modulus were obtained according to the force-displacement relationship of the compression test.

Fig. 8.B shows the experimental relative compressive effective elastic modulus by the approximate line that gives the effective elastic modulus E_{eff} =187.49 MPa. By using the elastic modulus E=110 GPa in Fig. 6.B, the E_{eff} is found to be 219.2 MPa. Compared to the experimental data, the analytical value is bigger, and error 16.7% has been found. This may due to the fact that the control of the strut diameter is very difficult and the toughness may have an influence too.

Specimen	Morphological characteristics			Mechanical properties of basic material	
RD lattice	Cuboid dimensions	$d_{\text{as designed}}$	$b_{\text{as designed}}$	Elastic modulus [GPa]	Poisson's ratio

structure	[mm]	[mm]	[mm]		
	24.6×24.6×28.2	0.5	5	110	0.3

Table 4 Morphological characteristics and mechanical properties of Ti-6Al-4V RD-lattice-structure specimen

4. References

[1] Gibson L J, Ashby M F. Cellular solids: structure and properties [M]. Cambridge university press, 1999.

[2] Takezawa A, Koizumi Y, Kobashi M. High-stiffness and strength porous maraging steel via topology optimization and selective laser melting [J]. Additive Manufacturing, 2017, 18: 194-202.

[3] Harrysson O L A, Cansizoglu O, Marcellin-Little D J, et al. Direct metal fabrication of titanium implants with tailored materials and mechanical properties using electron beam melting technology [J]. Materials Science and Engineering: C, 2008, 28(3): 366-373.

[4] Li Z, Wang K F, Wang B L, et al. The thermal shock resistance prediction of porous ceramic sandwich structures with temperature-dependent material properties [J]. Ceramics International, 2019, 45(3): 4043-4052.

[5] Lan X, Wang Z. Efficient high-temperature electromagnetic wave absorption enabled by structuring binary porous SiC with multiple interfaces[J]. Carbon, 2020, 170: 517-526.

[6] Klippstein H, Hassanin H, Diaz De Cerio Sanchez A, et al. Additive manufacturing of porous structures for unmanned aerial vehicles applications [J]. Advanced Engineering Materials, 2018, 20(9): 1800290.

[7] Bici M, Brischetto S, Campana F, et al. Development of a multifunctional panel for aerospace use through SLM additive manufacturing[J]. Procedia CIRP, 2018, 67: 215-220.

[8] Rodríguez-Montaño Ó L, Cortés-Rodríguez C J, Uva A E, et al. Comparison of the mechanobiological performance of bone tissue scaffolds based on different unit cell geometries [J]. Journal of the mechanical behavior of biomedical materials, 2018, 83: 28-45.

[9] Wang S, Zhou X, Liu L, et al. On the design and properties of porous femoral stems with adjustable stiffness gradient [J]. Medical Engineering & Physics, 2020.

[10] Sharma P, Jain K G, Pandey P M, et al. In vitro degradation behaviour, cytocompatibility and hemocompatibility of topologically ordered porous iron scaffold prepared using 3D printing and pressureless microwave sintering [J]. Materials Science and Engineering: C, 2020, 106: 110247.

[11] Chang C, Huang J, Yan X, et al. Microstructure and mechanical deformation behavior of selective laser melted Ti6Al4V ELI alloy porous structures [J]. Materials Letters, 2020, 277: 128366. [12] Li Y M, Hoang M P, Abbes B, et al. Analytical homogenization for stretch and bending of honeycomb sandwich plates with skin and height effects [J]. Composite Structures, 2015, 120: 406-416.

[13] Huang Y, Xue Y, Wang X, et al. Effect of cross sectional shape of struts on the mechanical properties of aluminium based pyramidal lattice structures [J]. Materials Letters, 2017, 202: 55-58.

[14] Yin H, Zheng X, Wen G, et al. Design optimization of a novel bio-inspired 3D porous structure for crashworthiness [J]. Composite Structures, 255: 112897.

[15] Hedayati R, Sadighi M, Mohammadi-Aghdam M, et al. Effect of mass multiple counting on the elastic properties of open-cell regular porous biomaterials [J]. Materials & Design, 2016, 89: 9-20

[16] Yan X, Li Q, Yin S, et al. Mechanical and in vitro study of an isotropic Ti6Al4V lattice structure fabricated using selective laser melting [J]. Journal of Alloys and Compounds, 2019, 782: 209-223.

[17] Bandyopadhyay A, Espana F, Balla V K, et al. Influence of porosity on mechanical properties and in vivo response of Ti6Al4V implants [J]. Acta biomaterialia, 2010, 6(4): 1640-1648.

[18] Murr L E, Esquivel E V, Quinones S A, et al. Microstructures and mechanical properties of electron beam-rapid manufactured Ti–6Al–4V biomedical prototypes compared to wrought Ti–6Al–4V [J]. Materials characterization, 2009, 60(2): 96-105

[19] Cao X, Duan S, Liang J, et al. Mechanical properties of an improved 3D-printed rhombic dodecahedron stainless steel lattice structure of variable cross section [J]. International Journal of Mechanical Sciences, 2018, 145: 53-63

[20] Yang L, Han C, Wu H, et al. Insights into unit cell size effect on mechanical responses and energy absorption capability of titanium graded porous structures manufactured by laser powder bed fusion [J]. Journal of the Mechanical Behavior of Biomedical Materials, 2020: 103843

[21] Horn T J, Harrysson O L A, Marcellin-Little D J, et al. Flexural properties of Ti6Al4V rhombic dodecahedron open cellular structures fabricated with electron beam melting [J]. Additive manufacturing, 2014, 1: 2-11

[22] Li F, Li J, Kou H, et al. Compressive mechanical compatibility of anisotropic porous Ti6Al4V alloys in the range of physiological strain rate for cortical bone implant applications [J]. Journal of Materials Science: Materials in Medicine, 2015, 26(9): 233.

[23] Babaee S, Jahromi B H, Ajdari A, et al. Mechanical properties of open-cell rhombic dodecahedron cellular structures [J]. Acta Materialia, 2012, 60(6-7): 2873-2885

[24] http://www.freelem.com/theorie/matrices_globales.htm

Annex:

For a bending beam deformed around *z*-direction, the nodal displacements and rotation angles are used as the unknown variables as shown in Fig. 9.

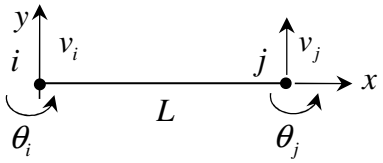

Fig. 9 beam element

By considering 4 boundary conditions on the two nodes of a beam, the displacement in the *Y*-direction for a beam in bending around *z*-direction is supposed to be a polynomial with 4 coefficients to determine as follows:

$$v(x) = ax^3 + bx^2 + cx + d \tag{A1}$$

With small elastic deformation, the rotation angle is supposed as follows:

$$\theta(x) \approx \tan\theta(x) = v'(x) = 3ax^2 + 2bx + c \tag{A2}$$

With the following boundary conditions:

$$v(0) = v_i;\ v(L) = v_j;\ \theta(0) = \theta_i;\ \theta(L) = \theta_j \tag{A3}$$

Using Eqs. (A2), (A3) and (A4):

$$v(x)=\begin{bmatrix}N_1 & N_2 & N_3 & N_4\end{bmatrix}\{u\} \tag{A4}$$

with $\Rightarrow \langle u\rangle=\{u\}^T=\langle v_i \;\; \theta_i \;\; v_j \;\; \theta_j\rangle$, and

$$N_1=1-3\bar{x}^2+2\bar{x}^3;\;\; N_2=L\left(\bar{x}-2\bar{x}^2+\bar{x}^3\right)$$

$$N_3=3\bar{x}^2-2\bar{x}^3;\;\; N_4=L\left(-\bar{x}^2+\bar{x}^3\right);\;\; \bar{x}=\frac{x}{L}$$

Strain energy of the beam is:

$$U=\frac{EI}{2}\int_0^L\left(\frac{\partial^2 v}{\partial x^2}\right)^2 dx \tag{A5}$$

And assuming the strain energy in form of matrix:

$$U=\frac{1}{2}\langle u\rangle[K]\{u\} \tag{A6}$$

Using Eq. (A5) in Eq. (A6), and comparing to Eq. (A7):

$$[K]=\frac{EI}{L^3}\begin{bmatrix}12 & 6L & -12 & 6L\\ & 4L^2 & -6L & 2L^2\\ & & 12 & -6L\\ & & & 4L^2\end{bmatrix} \tag{A7}$$

In which:

$$K_{ij}=K_{ji}=\int_0^L\frac{\partial^2 N_i}{\partial x^2}\frac{\partial^2 N_j}{\partial x^2}dx$$

The transformation from local coordinate system to global one is:

$$\begin{aligned}&[K]_l\{u\}_l=\{f\}_l\Rightarrow[R_C][K]_l\left([R_C]^T\{u\}\right)=[R_C]\left([R_C]^T\{f\}\right)\\ &\Rightarrow[R_C][K]_l[R_C]^T\{U\}=\{F\}\Rightarrow[K]_g=[R_C][K]_l[R_C]^T\end{aligned} \tag{A8}$$